Sixth International Symposium on Turbulence and Shear Flow Phenomena
Seoul, Korea, 22-24 June 2009

TURBULENT PRANDTL NUMBER IN A CHANNEL FLOW FOR *Pr* = 0.025 and 0.71

Hiroyuki Abe
Japan Aerospace Exploration Agency
Chofu, Tokyo 182-8522, Japan
habe@chofu.jaxa.jp

Robert Anthony Antonia
Discipline of Mechanical Engineering
University of Newcastle
NSW 2308, Australia
robert.antonia@newcastle.edu.au

ABSTRACT

DNS databases in a turbulent channel flow with passive scalar transport and a constant time-averaged heat-flux boundary condition have been used to examine the variation of the turbulent Prandtl number (Pr_t) across the channel. Two values of the molecular Prandtl number Pr are considered (0.025 and 0.71); in each case, data were obtained for four values of h^+ (180, 395, 640, 1020). For Pr=0.71, Pr_t is 1.1 at the wall, varies between 0.9 and 1.1 in the region $y^+ <100$, and is represented by $0.9 - 0.3(y/h)^2$ for $y/h >0.2$. The closeness to unity near the wall is attributed to the excellent similarity between the velocity and scalar fields, whereas the decrease in magnitude in the outer region is most likely associated with the unmixedness of the scalar. A similar description for Pr_t is not possible for Pr=0.025 due to the strong conductive effects. In this case, the near-wall limiting value is unlikely to approach unity.

INTRODUCTION

The turbulent Prandtl number, which is defined as the ratio of the turbulent eddy viscosity (ν_t) to the turbulent eddy diffusivity (a_t),

$$Pr_t = \frac{\nu_t}{a_t} = \frac{\overline{uv}}{\overline{v\theta}} \frac{\mathrm{d}\overline{\Theta}/\mathrm{d}y}{\mathrm{d}\overline{U}/\mathrm{d}y} \quad (1)$$

is an important quantity in the context of computing (e.g. via RANS and LES) turbulent shear flows with scalar transport (u, v, w denote the streamwise, wall-normal and spanwise velocity fluctuations, respectively, and θ is the temperature fluctuation. Upper case quantities represent instantaneous values; x, y, z are the streamwise, wall-normal and spanwise directions, respectively. An overbar denotes the averaged value with respect to space and time). However, its accurate measurement is difficult especially in the near-wall region (e.g. Launder 1976). Firm conclusions have hence not been formulated with respect to the detailed dependence of Pr_t on the Reynolds and Prandtl numbers and also the distance from the wall. Its value is sometimes assumed to be constant (viz. Pr_t=0.9). The closeness to unity implies a close similarity between the velocity and scalar fields. However, this similarity may break down when $Pr \ll 1$ or $Pr \gg 1$ (e.g. Reynolds 1975).

Direct numerical simulations (DNSs) have yielded accurate near-wall turbulence quantities, thus allowing significant improvement in near-wall turbulence models (e.g. Mansour et al. 1988). Antonia and Kim (1991) examined the near-wall behavior of Pr_t in a turbulent channel flow using the DNS database obtained from Kim and Moin (1988). Three values of Pr (0.1, 0.71 and 2) were examined at $h^+ \equiv u_\tau h/\nu$=180 (u_τ, h, ν denote the friction velocity, channel half-width and kinematic viscosity, respectively. A superscript + denotes normalization by wall units.). The near-wall limiting value was 1.1, almost independently of Pr. For other DNSs at low/moderate Reynolds numbers ($h^+ \leq 395$) (Kasagi and Ohtsubo 1993; Kawamura et al. 1999), the same wall limiting value was also reported for moderate but not very low values of Pr (e.g. Pr=0.025). However, it is not clear what happens at larger h^+ (i.e. h^+>395) and to what extent Pr_t varies throughout the channel. These issues need to be sorted out before further progress in turbulence scalar modelling can be made.

In the present study, we examine the behavior of Pr_t across the channel along with that of turbulent heat fluxes using the DNS databases by Abe et al. (2004, 2009). Four values of h^+ (180, 395, 640 and 1020) are investigated for two types of working fluid, namely mercury (Pr=0.025) and air (Pr=0.71). The main objective is to quantify this behavior and clarify the functional dependence of Pr_t with respect to h^+, Pr, and y. Attention is also given to turbulence modelling for a_t (e.g. Nagano and Kim 1988; Yoshizawa 1988), where the relationship between Pr_t and R (time-scale ratio) is discussed.

DNS DATABASES

The present databases have been obtained from DNSs in a turbulent channel flow with passive scalar transport for h^+= 180, 395, 640 and 1020 at Pr=0.025 and 0.71 by Abe et al. (2004, 2009). The thermal boundary condition employed is a constant time-averaged heat-flux (Kasagi et al. 1992; Kasagi and Ohtsubo 1993). The numerical methodology is briefly as follows. A fractional step method is used with semi-implicit time advancement. The Crank-Nicolson method is used for the viscous terms in the y direction and

Table 1 Domain size, grid points and spatial resolution.

h^+		180	395	640	1020
$L_x \times L_y \times L_z$		$12.8h \times 2h \times 6.4h$			
$L_x^+ \times L_y^+ \times L_z^+$		$2304 \times 360 \times 1152$	$5056 \times 790 \times 2528$	$8192 \times 1280 \times 4096$	$13056 \times 2040 \times 6528$
Pr=0.71	$N_x \times N_y \times N_z$	$768 \times 128 \times 384$	$1536 \times 192 \times 768$	$2048 \times 256 \times 1024$	$2048 \times 448 \times 1536$
	Δx^+, Δy^+, Δz^+	3.00, 0.20 ~ 5.93,3.00	3.29,0.15 ~ 6.52,3.29	4.00,0.15 ~ 8.02,4.00	6.38, 0.15 ~ 7.32, 4.25
Pr=0.025	$N_x \times N_y \times N_z$	$256 \times 128 \times 256$	$512 \times 192 \times 512$	$1024 \times 256 \times 1024$	$2048 \times 448 \times 1536$
	Δx^+, Δy^+, Δz^+	9.00,0.20 ~ 5.93,4.50	9.88,0.15 ~ 6.52,4.94	8.00,0.15 ~ 8.02,4.00	6.38, 0.15 ~ 7.32, 4.25

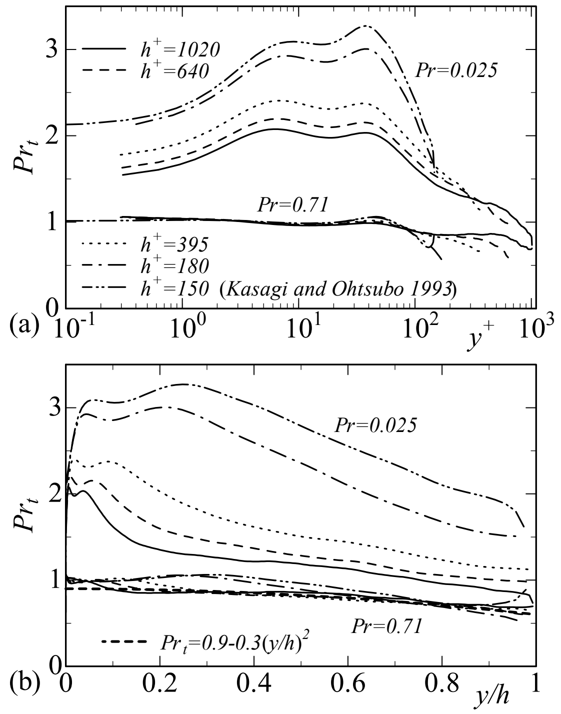

Figure 1: Distributions of Pr_t: (a) inner scaling; (b) outer scaling.

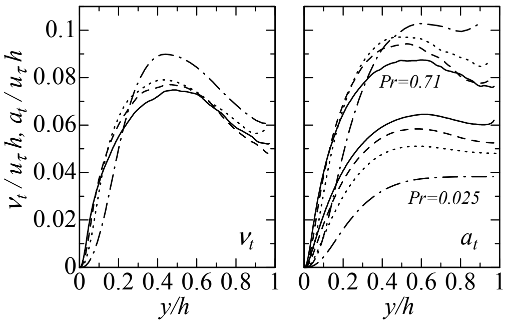

Figure 2: Distributions of ν_t and a_t normalized by outer variables.

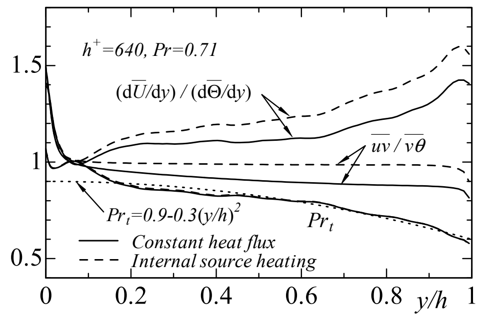

Figure 3: A comparison of Pr_t between the constant heat flux and internal source heating (h^+=640 and Pr=0.71).

the 3rd-order Runge-Kutta method for the other terms. Three exceptions are the cases for h^+= 180, 395 and 640 at Pr=0.025, where the 2nd-order Adams-Bashforth method is employed instead of the 3rd-order Runge-Kutta method. For the spatial discretization, a 4th-order finite difference central scheme is used in the x and z directions, with a 2nd-order central scheme in the y direction. Further details and validation of turbulence statistics can be found in Abe et al. (2004, 2009) and Antonia et al. (2009). The computational domain size ($L_x \times L_y \times L_z$), number of grid points ($N_x \times N_y \times N_z$) and spatial resolution (Δx, Δy, Δz) are given in Table 1. Note that for h^+=1020 the same velocity field has been used for computations at Pr=0.025 and 0.71, whereas for h^+=180, 395 and 640 different velocity fields have been used for simulations at each Pr. Also for the latter three h^+ at Pr=0.71, two scalar fields with different thermal boundary conditions (viz. the constant heat flux (Kasagi et al. 1992) and the internal source heating (Kim and Moin 1989)) have been time-advanced simultaneously with the same velocity field, where attention was given to small scales (Abe et al. 2009) so that the spatial resolution is finer than that for the other cases. A few results with the internal source heating are also included for comparison.

RESULTS AND DISCUSSION

Distributions of Pr_t , normalized by inner and outer variables, are shown in Fig. 1. For Pr=0.71, the inner and outer scalings are valid for y^+<100 and y/h>0.2, respectively. The wall limiting value is 1.1, independently of h^+, consistent with the finding of Antonia and Kim (1991) at h^+=180. For y^+ <100, Pr_t does not vary significantly; it remains in the range 0.9 to 1.1. In particular, the magnitude is large near the wall, which is attributed to the close analogy between the velocity and scalar fields (Antonia et al. 2009; Abe and Antonia 2009) (see also Fig. 4). The magnitude of Pr_t however decreases gradually towards the channel centerline (see a difference between ν_t and a_t in Fig. 2). In the outer region (y/h>0.2), the distributions are described approximately by

$$Pr_t = 0.9 - 0.3(y/h)^2 , \quad (2)$$

which is similar to the suggestion by Rotta (1964). Eq. (2) is also applicable when the heating is done with an internal source (see the almost perfect correspondence between the constant heat flux and the internal source heating in Fig. 3). Further, other DNS data (Kim and Moin 1988; Kawamura et al. 1998) indicate that Eq. (2) seems to apply not only for air but also for water (viz. Pr = 5 ~ 7).

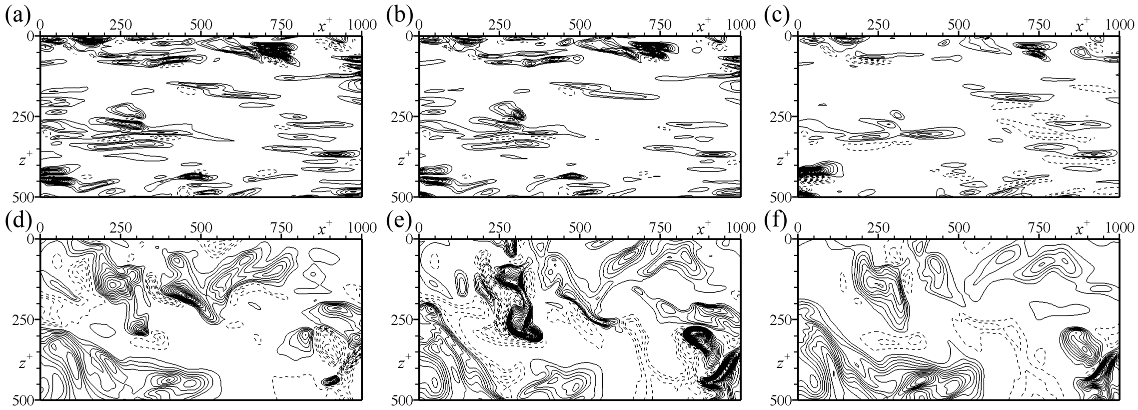

Figure 4: Contours of uv and $v\theta$ at h^+=1020: (a),(d) uv; (b),(e) $v\theta$ for Pr=0.71; (c),(f) $v\theta$ for Pr=0.025. For (a), (b) and (c), y^+=10 and for (d), (e) and (f), y/h=0.4. Solid and dashed lines are negative and positive values, respectively. Line increments for uv and $v\theta$ for Pr=0.71 are 0.5 independently of y, whilst those for $v\theta$ for Pr=0.025 are 0.025 and 0.25 at y^+=10 and y/h=0.4, respectively.

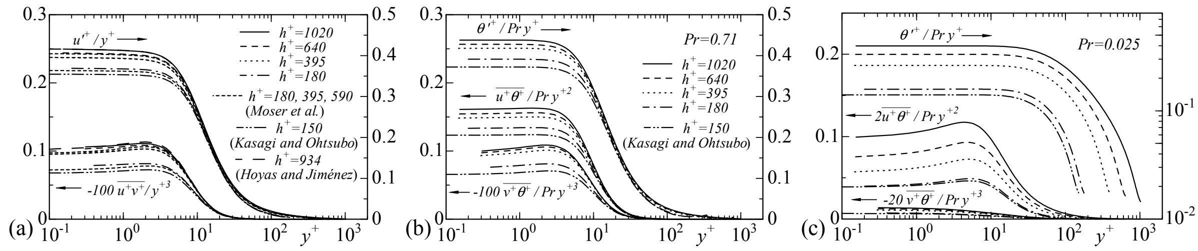

Figure 5: Near-wall limiting behavior for u', θ', $\overline{uv}$, $\overline{u\theta}$ and $\overline{v\theta}$.

The decrease in magnitude in the outer region is most likely to be associated with the unmixedness of the scalar (Guezennec et al. 1990; Antonia et al. 2009). In this context, $v\theta$ exhibits sharper interfaces than uv (see x^+=z^+=250 in Fig. 4), the difference being attributed to the unmixed nature of scalar (distributions of θ are not shown here). This leads to a discernible difference in the high wavenumber part of the co-spectra (not shown here), the $v\theta$ co-spectrum being more energetic than the uv co-spectrum. Such a difference appears as a small difference between $\overline{uv}$ and $\overline{v\theta}$ (note that $\overline{uv}\,/\,\overline{v\theta}$ <1 in Fig. 3), which is related to the difference between $\mathrm{d}\overline{U}/\mathrm{d}y$ and $\mathrm{d}\overline{\Theta}/\mathrm{d}y$ (see $\left(\mathrm{d}\overline{U}/\mathrm{d}y\right)/\left(\mathrm{d}\overline{\Theta}/\mathrm{d}y\right)$ >1 in Fig. 3) via the relations for the total shear stress and heat flux. The latter difference can also be discerned in the mean velocity and scalar distributions (not shown here), the gradient of the mean velocity being steeper than that for the mean scalar in the outer region.

For Pr=0.025, on the other hand, the strong conductive effects affect Pr_t noticeably. Whilst the magnitude decreases significantly with increasing h^+, the large departure from unity persists throughout the channel, implying a breakdown of the analogy between the velocity and scalar fields (see a large difference between ν_t and a_t in Fig. 2). Two local peaks appear at y^+ = 5 and 45. This is attributed to the difference between the mean velocity and scalar distributions. With regard to Fig. 4, although there is a relatively good similarity in $v\theta$ between Pr=0.025 and 0.71 in the outer region (the correlation coefficient between Figs. 4e and f is 0.81), the similarity is reduced near the wall (the correlation coefficient between Figs. 4b and c is 0.59). This is because near-wall thermal streaks are not noticeable for Pr=0.025. Instead, large-scale θ structures tend to stretch across both inner and outer regions (Kasagi and Ohtsubo 1993; Abe et al. 2004). Since the latter structures tend to be correlated with v, the near-wall correlation between θ and v is smaller for Pr=0.025 than Pr=0.71. Consistently, the magnitude of $\overline{v\theta}$ is smaller for Pr=0.025 than Pr=0.71 (see Figs. 5b and c). This would explain the near-wall departure of Pr_t from unity for Pr=0.025.

The difference in Pr_t between Pr=0.025 and 0.71 is examined further by investigating its near-wall limiting behavior. Taylor series expansions of $\overline{U_1}$, $\overline{\Theta}$, $\overline{uv}$, $\overline{v\theta}$ together with u', θ' and $\overline{u\theta}$ are expressed as follows:

$$\overline{U_1}^{+} = y^+ - \frac{y^{+2}}{2h^+} + O\left(y^{+4}\right), \tag{3}$$

$$\overline{\Theta}^{+} = Pr\left(y^+ - \frac{y^{+2}}{2h^+}\right) + O\left(y^{+4}\right), \tag{4}$$

$$u'^{+} = b_1' y^+ + c_1' y^{+2} + d_1' y^{+3} + O\left(y^{+4}\right), \tag{5}$$

$$\theta'^{+} = b_\theta' y^+ + d_\theta' y^{+3} + O\left(y^{+4}\right), \tag{6}$$

$$\overline{u^+v^+} = \overline{b_1c_2}\,y^{+3} + O\left(y^{+4}\right), \tag{7}$$

$$\overline{u^+\theta^+} = \overline{b_1b_\theta}\,y^{+2} + \overline{c_1b_\theta}\,y^{+3} + \left(y^{+4}\right), \tag{8}$$

$$\overline{v^+\theta^+} = \overline{c_2b_\theta}\,y^{+3} + O\left(y^{+4}\right), \tag{9}$$

where a prime denotes a rms value. With the use of Eqs. (3), (4), (7), (9), Pr_t may be written as

$$Pr_t = \frac{\overline{b_1c_2}}{\overline{c_2b_\theta}}Pr + O\left(y^+\right). \tag{10}$$

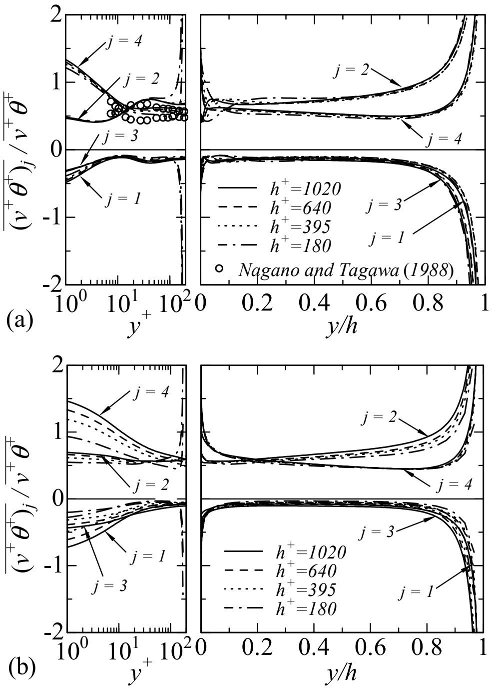

Figure 6: Quadrant analysis for $\overline{v\theta}$: (a) Pr=0.71; (b) Pr=0.025.

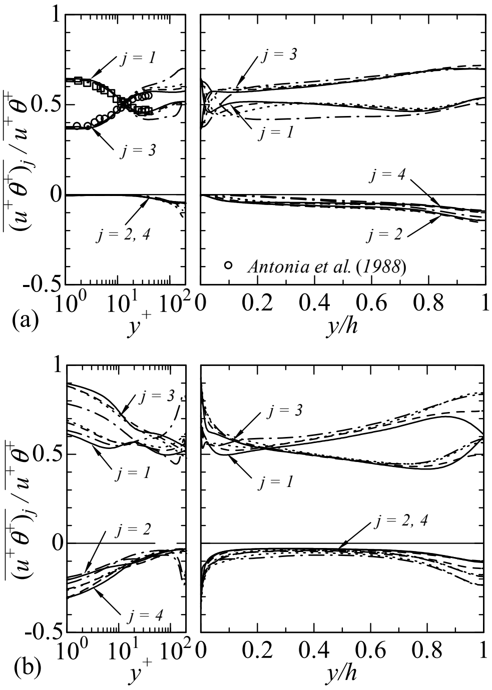

Figure 7: Quadrant analysis for $\overline{u\theta}$: (a) Pr=0.71; (b) Pr=0.025. Line patterns are the same as in Fig. 6.

Eq. (10) implies that the near-wall limiting value of Pr_t is determined by the relationship between $\overline{uv}$ and $\overline{v\theta}$. The distributions of $\overline{u^+v^+} / y^{+3}$ and $\overline{v^+\theta^+} / Pr\, y^{+3}$ together with u'^+ / y^+ and $\theta'^+ / Pr\, y^+$ are shown in Fig. 5, which highlights the leading order coefficients of the Taylor series expansions. Also included are the data of $\overline{u^+\theta^+} / Pr\, y^{+2}$. For Pr=0.71, the near-wall distributions of u' and $\overline{uv}$ are similar in shape to those of θ' and $\overline{v\theta}$, respectively, which is consistent with Pr_t = 1.1 independently of h^+. The rate of increase in the coefficients from h^+=180 to 395 is significant due to the low h^+ effects (Antonia and Kim 1994), whilst that from h^+=395 to 1020 is moderate (i.e. b_θ' / Pr =0.39, 0.42, 0.43, 0.44 at h^+=180, 395, 640, 1020, respectively). For Pr=0.025, on the other hand, the distributions of θ' and $\overline{v\theta}$ look quite different from those of u' and $\overline{uv}$, respectively, which is consistent with the large departure from unity of Pr_t. The magnitudes of the coefficients (viz. b_θ' , $\overline{b_1 b_\theta}$, $\overline{c_2 b_\theta}$) increase logarithmically with increasing h^+ (i.e. b_θ' / Pr =0.16, 0.26, 0.33, 0.40 at h^+=180, 395, 640, 1020, respectively). Antonia and Kim (1991) noted that the leading order coefficients for θ' , $\overline{u\theta}$ and $\overline{v\theta}$ tend to scale on Pr when $Pr \geq 0.1$. The same trend was also reported by Kawamura et al. (1998). However, this relationship is not applicable for Pr=0.025 (see Figs. 5b and 5c) due to the strong conductive effects. This result has important implications for turbulence modelling. Current models do not reflect the scaling on Pr (e.g. Nagano and Shimada 1996) correctly.

The above observations imply that there is a significant difference in the generation mechanism for turbulent heat-fluxes between Pr=0.025 and Pr=0.71. To clarify this issue, quadrant analysis has been applied to $\overline{v\theta}$ (Fig. 6). The latter method is often used to examine the generation mechanisms for the turbulent shear stress (Wallace et al. 1972; Willmarth and Lu 1972) and turbulent heat fluxes (Perry and Hoffmann 1976; Antonia et al. 1988). For Pr=0.71, the contributions from quadrants 2 and 4 are altered in the near-wall region ($y^+ \simeq 17$) and are almost similar to those for $\overline{uv}$ (not shown here). This implies a close similarity in the generation mechanism between $\overline{uv}$ and $\overline{v\theta}$ (see also Fig. 4). The distributions are normalized by inner and outer variables in the regions y^+<100 and y/h>0.2, respectively, as in the case of Pr_t . In contrast, when Pr=0.025, the contributions from quadrants 2 and 4 are changed in the outer region (y/h>0.2). Also a significant h^+ effect appears across the channel, consistent with the noticeable dependence of $\overline{v\theta}$ on h^+ (this is not shown here). A difference in generation mechanism between Pr=0.025 and 0.71 is hence likely in the region y/h<0.2.

The same Pr dependence is observed for $\overline{u\theta}$ (see Fig. 7), where the scaling range is nearly the same as for $\overline{v\theta}$ (see Figs. 6 and 7). For Pr=0.71, the contributions are indeed from quadrants 1 and 3 near the wall, implying a close similarity between u and θ (see also Abe and Antonia 2009). For Pr=0.025, on the other hand, the contributions from quadrants 2 and 4 cannot be dismissed near the wall, suggesting a breakdown of the analogy between u and θ. It hence follows that in the region y/h <0.2 turbulent heat fluxes for Pr=0.025 are generated in a different manner than for Pr=0.71.

The previous considerations imply that, as h^+ increases, the near-wall value of Pr_t for Pr=0.025, is unlikely to approach that which corresponds to Pr=0.71. It is however likely that it may reach it in the outer region. This latter

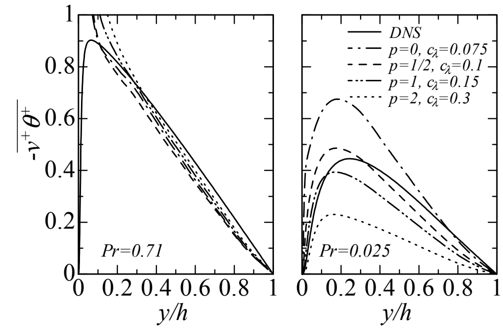

Figure 8: Evaluation of Eq. (14) at h^+= 1020.

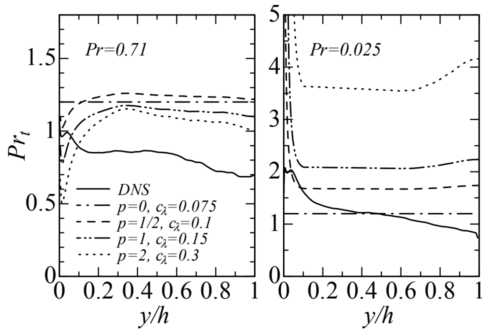

Figure 9: Evaluation of Eq. (17) at h^+= 1020.

expectation appears to be supported by the experimental evidence in turbulent pipe flows which indicates that, in the logarithmic region, the magnitude of Pr_t is nearly the same for Pr=0.025 and Pr=0.71 (see Table 1 of Kader and Yaglom 1972).

Finally, attention is given to turbulence models for a_t (Nagano and Kim 1998; Yoshizawa 1998). The standard ν_t and a_t models may be written as

$$\nu_t = c_\mu f_\mu \frac{k^2}{\varepsilon} , \qquad (11)$$

$$a_t = c_\lambda f_\lambda \frac{k^2}{\varepsilon} R^p , \qquad (12)$$

where

$$R = \frac{k_\theta / \varepsilon_\theta}{k / \varepsilon} \qquad (13)$$

(k, ε, k_θ , ε_θ and R denote the turbulent kinetic energy, the mean energy dissipation rate, the temperature variance and the mean scalar dissipation rate and the time scale ratio, respectively) (see also Horiuti 1992). Nagano and Kim (1988) used p=1/2, whilst Yoshizawa (1988) used p=2. Note that p=0 corresponds to Pr_t = constant. In the present flow, Eq. (12) can also be expressed as

$$-\overline{v\theta} = c_\lambda f_\lambda \frac{k^2}{\varepsilon} R^p \frac{d\overline{\Theta}}{dy} \qquad (14)$$

Eq. (14) is tested against the DNS data for h^+=1020 in Fig. 8, in order to ascertain the optimal value of p. Note that f_λ=1 and different values of c_λ are used for different p's to minimize differences between predictions for Pr=0.71 and the DNS distribution. In Eq. (14), the prediction with p=1/2 (Nagano and Kim 1988) is closest to the DNS data for both Prandtl numbers. The same trend has been also found for other h^+ (the distributions are not shown here). For p=1/2, Eq. (12) may readily be rewritten as

$$a_t = c_\lambda f_\lambda k \tau_m \qquad (15)$$

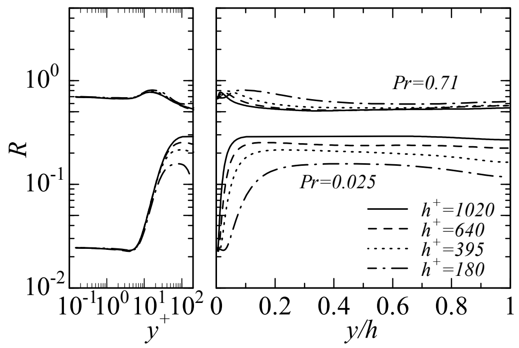

Figure 10: Distributions of R.

where

$$\tau_m = \left(\frac{k}{\varepsilon} \cdot \frac{k_\theta}{\varepsilon_\theta} \right)^{1/2} , \qquad (16)$$

i.e. the velocity and scalar time scales appear via their geometric mean. The present results indicate that Eq. (12) shows promise when predicting the mean scalar distribution for very low Pr fluid. Nonetheless, there is a discernible deviation from the DNS data even when p=1/2. Using the a_t model, Pr_t , or the ratio of Eqs. (11) and (12),

$$Pr_t = \frac{c_\mu f_\mu}{c_\lambda f_\lambda} R^{-p} \qquad (17)$$

(see also Antonia et al. 2009) deviates significantly from the DNS distribution (Fig. 9), where f_μ=1 and c_μ=0.09 are used. The relationship between Pr_t and R , as given by Eq. (17), does not hold in the outer region. This is because, unlike Pr_t, R is approximately constant for both Pr=0.025 and 0.71 (see Figs. 1 and 10). It seems likely that the use of a model function and/or the incorporation of a new time scale (e.g. Nagano and Shimada 1996) should reduce the deviation between the model and the DNS data. It should also be noted that for Pr=0.025, R, like Pr_t, is likely to approach the value corresponding to Pr=0.71 (viz. R=0.5) in the outer region.

CONCLUSIONS

The behaviour in a turbulent channel flow of Pr_t and the turbulent heat-fluxes has been examined using DNS databases for h^+=180, 395, 640 and 1020 at Pr=0.025 and 0.71 with a constant time-averaged wall heat flux condition (Abe et al. 2004, 2009). The main conclusions are

(1) For Pr=0.71, Pr_t is described in a piecewise manner, viz. i) it is 1.1 at the wall, ii) it varies between 0.9 and 1.1 in the region y^+ <100, and iii) it can be approximated by $0.9 - 0.3(y/h)^2$ for y/h >0.2. This description also applies when the heating is via an internal source. Eq. (2) is likely to apply to water as well as air. The closeness of Pr_t to unity near the wall is attributed to the close similarity between the velocity and scalar fields, whereas the decrease in magnitude in the outer region is most likely to be associated with the unmixedness of the scalar.

(2) For Pr=0.025, Pr_t cannot be described in the same way as for Pr=0.71 due to the strong conductive effects. There is a persistently large departure from unity of Pr_t

throughout the channel, as well as a noticeable dependence on h^+. Near the wall, θ is more poorly correlated with v than for Pr=0.71, which is consistent with the departure from unity of Pr_t. In this context, the near-wall limiting behaviour has shown that contrary to Pr=0.71, the coefficients $b_\theta{}'$, $\overline{b_1 b_\theta}$, $\overline{c_2 b_\theta}$ for Pr=0.025 do not scale on Pr. This should be taken into account when developing turbulence models.

(3) The quadrant analysis indicates that $\overline{u\theta}$ and $\overline{v\theta}$ are generated in different manners in the region y/h <0.2 between Pr=0.025 and Pr=0.71. This implies that, as h^+ increases, the magnitude of Pr_t for Pr=0.025 is not likely to approach that for Pr=0.71 in the near-wall region, although it is likely to attain it in the outer region.

(4) Existing models for a_t were tested against the DNS data for h^+=1020 for Pr=0.025 and 0.71. The p=1/2 model of Nagano and Kim (1988) provides the closest agreement with the DNS data. However, the relationship between Pr_t and R given by Eq. (17) does not hold in the outer region.

ACKNOWLEDGEMENTS

Computations performed on Numerical Simulator III at the Computer Centre of the Japan Aerospace Exploration Agency are gratefully acknowledged. We also thank Prof. Kawamura at Tokyo University of Science for his encouragement during the course of this work. HA was partially supported by the Ministry of Education, Culture, Sports, Science and Technology of Japan, Grant-in-Aid for Young Scientists (B), 20760125, 2009. RAA acknowledges the support of the Australian Research Council.

REFERENCES

Abe, H., Kawamura, H. and Matsuo, Y., 2004, "Surface heat-flux fluctuations in a turbulent channel flow up to Re_τ =1020 with Pr=0.025 and 0.71," Int. J. Heat and Fluid Flow Vol. 25, pp. 404-419.

Abe, H., Antonia, R.A. and Kawamura, H., 2009, "Correlation between small-scale velocity and scalar fluctuations in a turbulent channel flow," J. Fluid Mech., to appear.

Abe, H. and Antonia, R.A., 2009, "Near-wall similarity between velocity and scalar fluctuations in a turbulent channel flow," Phys. Fluids, Vol. 21, 025109.

Antonia, R.A. and Kim, J., 1991, "Turbulent Prandtl number in the near-wall region of a turbulent channel flow," Int. J. Heat Mass Transfer, Vol. 34(7), pp. 1905-1908.

Antonia, R.A. and Kim, J., 1994, "Low-Reynolds-number effects on near-wall turbulence," J. Fluid Mech. Vol. 276, pp. 61-80.

Antonia, R.A., Krishnamoorthy, L. V. and Fulachier, L. 1988, "Correlation between the longitudinal velocity fluctuation and temperature fluctuation in the near-wall region of a turbulent boundary layer," Int. J. Heat Mass Transfer, Vol. 31(4), pp. 723-730.

Antonia, R.A., Abe, H. and Kawamura, H., 2009, "Analogy between velocity and scalar fields in a turbulent channel flow," J. Fluid Mech., to appear.

Guezennec, Y., Stretch. D. and Kim, J., "The structure of turbulent channel flow with passive scalar transport," Proceedings of the 1990 Summer Program of Centre for Turbulence Research (NASA Ames/Stanford University, Stanford, CA, 1990), pp. 127-138.

Horiuti, K., 1992, "Assessment of two-equation models of turbulent passive-scalar diffusion in channel flow," J. Fluid Mech. Vol. 238, pp. 405-433.

Hoyas, S. and Jiménez, J. 2008 "Reynolds number effects on the Reynolds-stress budgets in turbulent channels," Phys. Fluids, Vol. 20, 101511.

Kader, B.A. and Yaglom, A.M., 1972, "Heat and mass transfer laws for fully turbulent wall flows," Int. J. Heat Mass Transfer, Vol. 15, pp. 2329-2351.

Kasagi, N. Tomita, Y. and Kuroda, A., 1992, "Direct numerical simulation of passive scalar field in a turbulent channel flow," ASME J. Heat Transfer, Vol. 114, pp. 598-606.

Kasagi, N. and Ohtsubo, Y., 1993, "Direct numerical simulation of low Prandtl number thermal field in a turbulent channel flow," In: Turbulent Shear Flows 8 (Edited by Durst et al.), pp. 97-119, Springer, Berlin.

Kawamura, H., Ohsaka, K., Abe, H. and Yamamoto, K., 1998, "DNS of turbulent heat transfer in channel flow with low to medium-high Prandtl number fluid," Int. J. Heat Fluid Flow, Vol. 19, pp. 482-491.

Kawamura, H., Abe, H. and Matsuo, Y., 1999, "DNS of turbulent heat transfer in channel flow with respect to Reynolds and Prandtl number effects," Int. J. Heat Fluid Flow, Vol. 20, pp. 196-207.

Kim, J. and Moin. P. 1989, "Transport of passive scalars in a turbulent channel flow," In: Turbulent shear flows 6 (Edited by André et al.), pp. 85-96, Springer, Berlin.

Launder, B.E., 1976, "Heat and Mass Transport, Topics in Applied Physics," Vol. 12, pp. 231-287.

Mansour, N.N., Kim, J. and Moin, P., 1988, "Reynolds-stress and dissipation-rate budgets in a turbulent channel flow," J. Fluid Mech., Vol. 194, pp. 15-44.

Moser, R.D., Kim, J. and Mansour, N.N., 1999 "Direct numerical simulation of turbulent channel flow up to Re_τ = 590," Phys. Fluids, Vol. 11, pp. 943-945.

Nagano, Y. and Kim, C., 1988, "A two-equation model for heat transport in wall turbulent shear flows," ASME J. Heat Transfer, Vol. 110, pp. 583-589.

Nagano, Y. and Shimada, M., 1996, "Development of a two-equation heat transfer model based on direct simulations of turbulent flows with different Prandtl numbers," Phys. Fluids., Vol. 8, pp. 3379-3402.

Nagano, Y. and Tagawa, M., 1988, "Statistical characteristics of wall turbulence with a passive scalar," J. Fluid Mech., Vol. 196, pp. 157-185.

Perry, E. and Hoffmann, P. H., 1976, "An experimental study of turbulent convective heat transfer from a flat plate," J. Fluid Mech. Vol. 77, pp. 355-368.

Reynolds, A.J., 1975, "T The prediction of turbulent Prandtl and Schmidt numbers," Int. J. Heat Mass Transfer, Vol. 18, pp. 1055-1069.

Rotta, J.C., 1964, "Temperaturverteilungen in der turbulenten grenzschicht an der ebenen platte," Int. J. Heat Mass Transfer, Vol. 7, pp. 215-228.

Wallace, J. M., Eckelmann, H. and Brodkey, R. S., 1972, "The wall region in turbulent shear flow," J. Fluid Mech. Vol. 54, pp. 39-48.

Willmarth, W. W. and Lu, S. S., 1972, "Structures of the Reynolds stress near the wall," J. Fluid Mech. Vol. 55, pp. 65-92.

Yoshizawa, A., 1988, "Statistical modelling of passive-scalar diffusion in turbulent shear flows," J. Fluid Mech. Vol. 195, pp. 541-555.